

V. A. Alexeev · P. L. Langen · J. R. Bates

Polar amplification of surface warming on an aquaplanet in “ghost forcing” experiments without sea ice feedbacks

Received: 15 November 2004 / Accepted: 17 February 2005
© Springer-Verlag 2005

Abstract Polar amplification of surface warming has previously been displayed by one of the authors in a simplified climate system model with no ice-albedo feedbacks. A physical mechanism responsible for this pattern is presented and tested in an energy balance model and two different GCMs through a series of fixed-SST and “ghost forcing” experiments. In the first ghost forcing experiment, 4 W/m^2 is added uniformly to the mixed layer heat budget and in the second and third, the same forcing is confined to the tropics and extra-tropics, respectively. The result of the uniform forcing is a polar amplified response much like that resulting from a doubling of CO_2 . Due to an observed linearity this response can be interpreted as the sum of the essentially uniform response to the tropical-only forcing and a more localized response to the extra-tropical-only forcing. The flat response to the tropical forcing comes about due to increased meridional heat transports leading to a warming and moistening of the high-latitude atmosphere. This produces a longwave forcing on the high-latitude surface budget which also has been observed by other investigators. Moreover, the tropical surface budget is found to be more sensitive to SST changes than the extra-tropical surface budget. This strengthens the tendency for the above mechanism to produce polar amplification, since the tropics need to warm less to counter an imposed forcing.

1 Introduction

Most of the existing coupled ocean-atmosphere models produce polar amplified surface warming of different intensity in $2\times\text{CO}_2$ experiments (Houghton et al. 2001). Interestingly, the same models display the largest disagreement in the polar regions (Walsh et al. 2002) and much research is still needed before we can claim to fully understand the climate system’s response to any type of forcing. One can define a pattern of global warming based on the SST tendency; a definition based on the transient behavior. When viewed in the transient sense, the signal of global warming may well be greater in the areas of sea ice retreat than in the ice covered areas (Polyakov et al. 2002), especially at the beginning of the typical climate change runs with 1% per year CO_2 increase. Likewise, the response can be somewhat different in areas of deep convection because of the large heat capacity of the ocean (Manabe et al. 1991), especially if we view the signal in the transient sense. Quite different results can be found from the equilibrium response (e.g. Sokolov and Stone 1998), corresponding roughly to the end of $2\times\text{CO}_2$ integrations through gradual 1% yearly CO_2 increases. In the present article the global warming is studied as a stationary response to a doubled CO_2 concentration. Hence, the term *polar amplification* will designate the pattern of greater warming at high latitudes compared to the rest of the globe in this stationary response.

Feedbacks associated with sea ice and snow cover are widely accepted as being the main cause of the polar amplification (e.g., Hansen et al. 1997; Hall 2004). In the simplest case of purely thermodynamic sea ice, both retreat and thinning of the ice will lead to surface warming. In a more complete framework with sea ice dynamics, however, other effects such as heat transport through leads and polynyas and ice motion may modify the picture (e.g., Hibler 1985; Flato and Hibler 1992; Vavrus and Harrison 2003).

V. A. Alexeev (✉)
International Arctic Research Center,
University of Alaska Fairbanks,
930 Koyukuk Dr., P. O. Box 757340, Fairbanks,
AK, 997757340 USA

P. L. Langen
Niels Bohr Institute, University of Copenhagen,
Juliane Maries Vej 30, 2100 Copenhagen O, Denmark

J. R. Bates
Mathematical Physics Department,
University College Dublin,
Belfield, Dublin 4, Ireland

Given the importance of sea ice for the polar regions, the significant polar amplification pattern in the system with no sea ice-albedo feedback obtained in Alexeev (2003) (hereinafter referred to as A03) seems to be a rather remarkable result. It suggests that there are feedbacks other than those associated with ice and snow albedo that affect the polar amplification.

Polar amplification in ocean-atmosphere systems without the ice-albedo effect has, to the best of the authors’ knowledge, not received much attention, although it has been seen in both energy balance models (e.g., Chen et al. 1995) and in GCM studies (Schneider et al. 1997, 1999). Bates (2003) has analyzed the stronger response to $2\times\text{CO}_2$ in the extra-tropics in a simple box model of the climate system including certain effects of atmospheric dynamics. The present study focuses on the mechanisms unrelated to sea ice and snow effects that contribute to the polar amplification. All effects of sea ice (e.g., albedo, dynamics, leads and complex rheology) are thus excluded in the configurations employed.

When analyzing the $2\times\text{CO}_2$ forcing it is calculated at the surface, rather than at the top of the atmosphere (TOA). Working in terms of the surface budget seems in our case more appropriate than in terms of the TOA budget, since the SST directly “feels” only the surface heat budget. The interaction between the surface budget and the atmospheric circulation has been discussed in a number of papers (e.g. Sarachik 1978; Bates 1999; Alexeev and Bates 1999; Alexeev 2003; Bellon et al. 2003).

Our system’s final equilibrium response has been found not to depend on the order of how the external forcing is applied, and the sensitivity experiment can therefore be carried out in two stages. During the first stage, an external forcing (e.g., doubling the CO_2 concentration) is instantaneously applied while the SST is kept fixed. This will allow the atmosphere to equilibrate, i.e., the global net imbalances at the surface and TOA will equal each other in the long term mean. The system as a whole may not be in equilibrium; there may be a non-zero net tendency on the SST. At this point the second stage of the sensitivity experiment is commenced and the SST is allowed to vary. With a mixed-layer depth of 50 m and a forcing of about 4 W/m^2 , an estimate for the typical time scale of the large scale mixed-layer readjustment is about 1.5–2 years. This provides the atmosphere with enough time to reach quasi-equilibrium with the SST, and the “fixed SST” strategy for calculating the total forcing on the climate system has proven a useful diagnostic tool, and has been successfully applied in A03 and Shine et al. (2003). Shine et al. (2003) demonstrated that using the total forcing calculated with fixed SST gives better results in sensitivity experiments with various forcings.

Another advantage of using the total surface forcing while keeping the SST fixed lies, as demonstrated by A03, in the possibility of studying the composition of the forcing in detail. Such an analysis of the total surface forcing and its components was performed in A03 for a

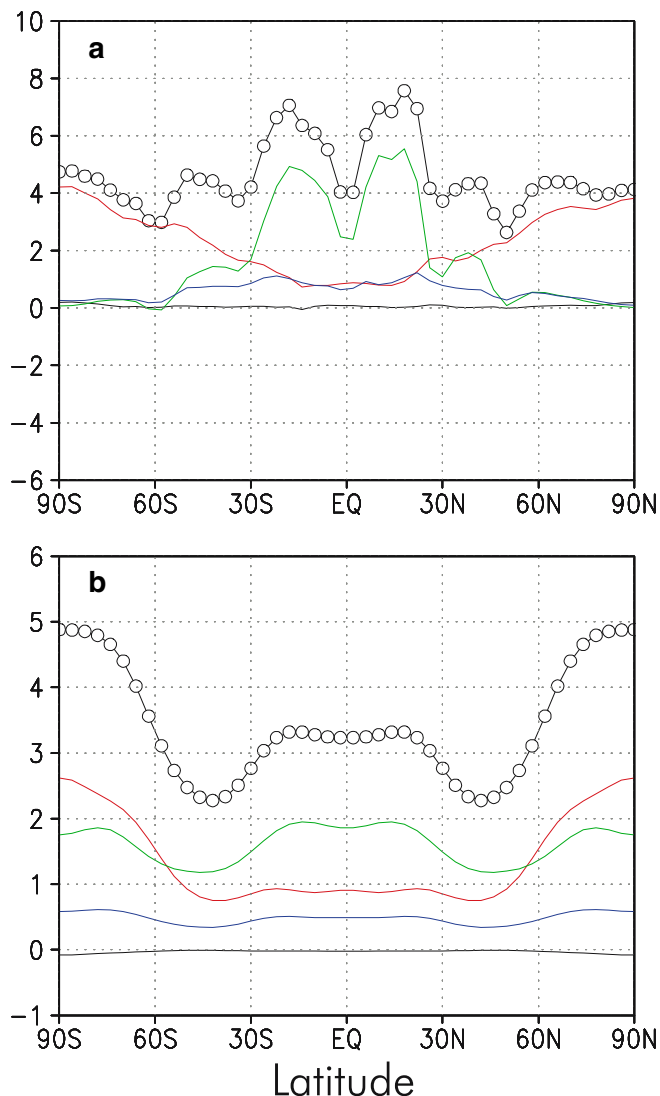


Fig. 1 **a** Total $2\times\text{CO}_2$ forcing at the surface (black circles) and its components—latent heat flux (green), longwave radiation (red), sensible heat flux (blue) and shortwave radiation (black). Units are W/m^2 . **b** SST response to the forcing from (a) and its individual components (same color code). Units are K. This is a reproduction of Fig. 9 from A03 and both panels are thus for Model 1 only

doubling of CO_2 . Figure 1 is a reproduction of Fig. 9 from A03 with opposite sign convention (positive forcing leads to warming). In addition, the response of the SST to each individual component of the total surface forcing was calculated. As noted in A03 (see Fig. 7b in A03), the linear estimate obtained compares very well with the full 3D $2\times\text{CO}_2$ run. The response to the latent heat flux component of the total surface forcing, which has significant magnitude only in the tropics, is very non-local and spreads out to the poles almost uniformly. The shape of the longwave radiative forcing and the corresponding SST response give the shape of the polar amplification of the $2\times\text{CO}_2$ warming. These findings are key to the present idea of using the “ghost forcing” approach for diagnosing the polar amplification pattern.

It is suggested here that the polar amplification pattern is the only possibility for our model climate systems to respond to any type of more or less uniform surface forcing. Initially, the low and high latitudes will respond similarly giving a uniformly increasing surface temperature. Such a temperature increase will lead to an increased meridional heat transport and, in turn, an increase in the high-latitude tropospheric temperature and specific humidity. This will increase the downwelling longwave flux at high latitudes and yield enhanced warming there. Even though the polar amplified response will eventually reduce the increased heat transport—perhaps even *counter* it—once equilibrium is approached, the initial increase rules out a uniform or *equatorially amplified* response.

This idea is discussed further in the next section within the framework of simple energy balance models. In Sect. 3 the robustness of the qualitative picture is demonstrated in two completely different GCMs. Three “ghost forcing” experiments (Hansen et al. 1997) are carried out as outlined in Table 1: a tropical surface forcing applied to the area within 30S to 30N, an extra-tropical forcing applied to the areas poleward of 30S/30N and a uniform forcing applied everywhere on the globe. It is shown that the response to the latter can be viewed as the sum of responses to the former two. The high-latitude forcing results in a local response while the low-latitude forcing, in accordance with the above mechanism, yields a near-uniform response and the result is a polar amplified warming. We also conduct experiments with fixed SST anomalies that illustrate how the polar regions feel the tropical SST change, an effect also observed by e.g., Schneider et al. (1997) and Rodgers et al. (2003).

2 EBM experiments

To study the polar amplification of surface warming in the simplest possible setting an energy balance model (EBM) of the Budyko-Sellers type is employed. The energy balance equation as given by North (1975) is:

$$\frac{d}{dx}D(1-x^2)\frac{d}{dx}T(x) = A + BT(x) - QS(x)(1-\alpha(x)), \quad (1)$$

where T is the zonally averaged surface temperature, D is a diffusion coefficient, A and B give the linear

parameterization of the outgoing longwave radiation at the TOA, Q is a fourth of the solar constant, S is an annually averaged heating function and α is the latitude-dependent TOA albedo. The latitude coordinate, x , is the sine of the latitude and the operator on the left hand side is the Laplacian in this coordinate. S is expressed in terms of a two-mode Legendre polynomial as $S(x) = 1 + S_2(3x^2 - 1)/2$, where $S_2 = -0.482$ yields a reasonable fit to the annually averaged heating function. The values $A = 205 \text{ W/m}^2$, $B = 2 \text{ W/m}^2\text{K}$ and $Q = 340 \text{ W/m}^2$ were chosen and the temperature is measured in degrees Celsius. When the albedo is variable (it will in some of what follows be kept fixed) it takes on the value 0.3 where T is $> -10 \text{ C}$ and 0.6 where T is $< -10 \text{ C}$. This permits the model to include the ice-albedo feedback (IAF). With these parameters the diffusion coefficient, D , is tuned and with a value of 0.445 the model equilibrates with the temperature profile shown in Fig. 2a (here T is shown in Kelvin).

In this equilibrium the three ghost forcing experiments are performed by simply adding an extra forcing term on the right hand side of the above energy balance equation. The outcome is shown in Fig. 2b for an active IAF: The black curve shows the equilibrium temperature increase in Exp1 while the red and green curves show the increases in Exp2 and Exp3, respectively. The blue curve shows the sum of the increases in Exp2 and Exp3. A number of features are evident: (1) All three experiments display a significant polar amplification, (2) Exp3 yields a greater amplification than Exp2 and (3) the result of Exp1 cannot be calculated as the sum of Exp2 and Exp3 as is the case for the forcings.

In an attempt to reproduce the result of polar amplification without the IAF, the surface albedo profile is fixed corresponding to the equilibrium found previously. The non-linearity of the albedo step function has now been eliminated from the energy balance equation rendering it linear in T . This is evident in Fig. 2c, which shows the result of repeating the three ghost forcing experiments: the warming in Exp1 equals the sum of the warmings in Exp2 and Exp3. There is no polar amplification in this case since B is constant with latitude leading to uniform increases in T . Uniform increases in T do not change the gradients and the meridional heat transports thus remain unchanged. Since the albedo is unchanged, the value of the uniform increase can be calculated as $4 \text{ W/m}^2/B = 2 \text{ K}$.

Exp2 and Exp3 both show amplified local warming and the global averaged warmings are in both cases $4 \text{ W/m}^2/B/2 = 1 \text{ K}$, since again the albedo is unchanged and the meridional transports only redistribute the heat (we divide by 2 since only half of the Earth’s area is being forced in Exp2 and Exp3). Since their sum equals 2 K everywhere, the two curves are each others’ mirror images about the line $T = 1 \text{ K}$. In fact, the local warmings (tropical average warming in Exp2 and extra-tropical average in Exp3) are equal and the same holds for the non-local warmings. This stems from the linearity of the energy balance equation: an anomalous

Table 1 Description of the three ghost forcing experiments performed with all models

Experiment	Area		Forcing (W/m ²)
Exp1	Global	90S to 90N	4
Exp2	Tropics	30S to 30N	4
Exp3	Extra-tropics	90S to 30S and 30N to 90N	4

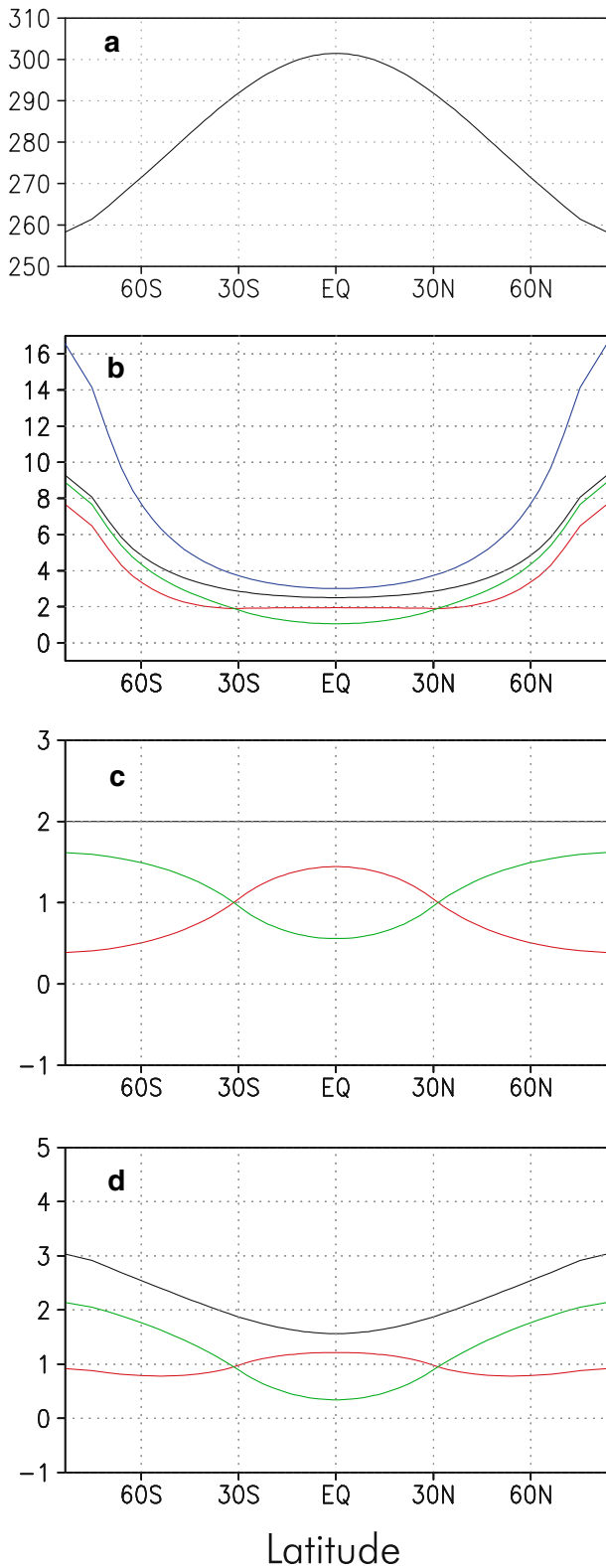


Fig. 2 Results from the EBM experiments: **a** Equilibrium SST. **b** SST increase in Exp1 (black), Exp2 (red), Exp3 (green) and sum of responses in Exp2 and Exp3 (blue); constant diffusion coefficient and active ice-albedo feedback. **c** As in (b), for experiments with inactive ice-albedo feedback and constant diffusion coefficient. The sum of increases in Exp2 and Exp3 is not plotted, since it coincides exactly with the increase in Exp1. **d** As in (c), but for the experiments with global SST dependent diffusion coefficient. Units are K

effect which is not modeled by the EBM with a constant diffusion coefficient is the increase in latent heat transport by a warmer atmosphere: a warmer atmosphere holds more moisture and with unchanged temperature gradient and eddy activity more heat will be transported polewards. This is demonstrated in Fig. 3 showing the change in heat transport resulting from a 1 K globally uniform increase in SST (results for one of the GCMs is shown here but heat transport changes will be discussed further for both models later). The black curve shows the total heat transport change as implied by the TOA and surface heat budgets while the red curve is the latent heat contribution implied by the surface freshwater budget (precipitation minus evaporation). The large peaks on the red curve in the tropics are due to an increase in the Hadley circulation. This increases the equatorward latent heat transport at low latitudes which, however, is largely compensated by a similar increase in the poleward dry static energy transport in the upper branch of the Hadley cell. The increase in mid-latitude heat transport, which we are interested in when studying tropical-extra-tropical interactions, is seen to come about chiefly due to the latent heat transport change.

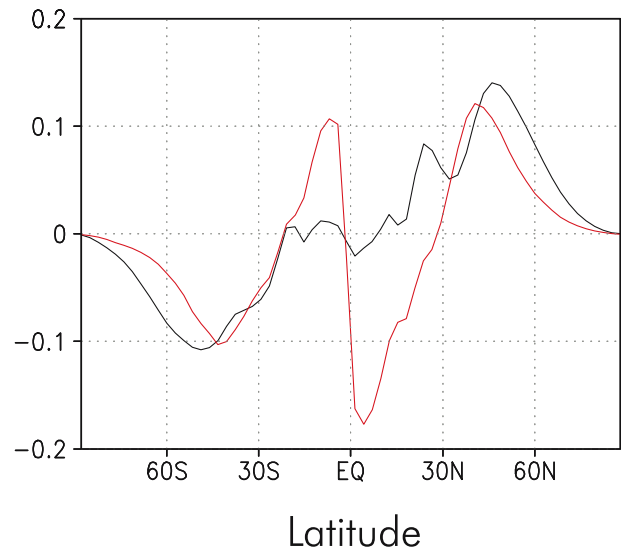


Fig. 3 Increase in the meridional heat transport (black) and the latent contribution thereto (red) in a uniform 1 K SST increase experiment. This figure shows results for Model 2 but changes in heat fluxes are shown for both models in Fig. 10. The two curves are inferred from the TOA—surface heat budget and the surface freshwater budget ($P-E$), respectively. Units are PW

temperature sets up an anomalous transport out of the forced area which is the same in both experiments. The symmetric way in which the tropics and extra-tropics are treated excludes the polar amplification.

This symmetry is not present in the GCMs which, as will be shown, do produce a polar amplification. One

This effect can crudely be included in our EBM by letting the diffusion coefficient be given as:

$$D(T_M) = D_{\text{ref}} \cdot [1 + r \cdot (T_M - T_{\text{ref}})], \quad (2)$$

where $D_{\text{ref}} = 0.445$ and $T_{\text{ref}} = 15$ C represent the diffusion coefficient and global mean temperature in the above equilibrium. T_M is the global mean temperature and r is the derivative of the heat transport with respect to T_M (normalized by D_{ref}). An illustrative value of 3%/K is chosen for this parameter which is in consistency with the increase seen in Fig. 3. It is, however, still a crude estimate in a crude parameterization, but while the magnitudes in the following naturally depend on the chosen value, the mechanism remains qualitatively invariant.

With this variable diffusion coefficient the above symmetry is broken: While earlier an increase of temperature in a zone lead only to an anomalous transport out of this zone, a temperature increase now leads to increased poleward transport in addition to the anomalous transport associated with the gradient changes. This leads to polar amplification of the warming as seen in Fig. 2d. While the symmetry between the tropics and the extra-tropics is broken, the linearity of the energy balance equation still holds and the response in Exp1 equals the sum of the responses in Exp2 and Exp3. The polar amplification arises as a result of a pronounced local response to the extra-tropical forcing and an essentially uniform global response to the tropical forcing.

In conclusion, it has been found that with a fixed diffusion coefficient leaving meridional transports dependent only on the temperature gradient no polar amplification of the warming signal is seen unless the ice-albedo feedback is included. Letting the diffusion coefficient increase with global mean temperature to crudely include effects of a warmer and moister atmosphere, polar amplification is, however, seen without the ice-albedo feedback. As long as the ice-albedo feedback is excluded the system responds linearly to the various ghost forcings such that the response in Exp1 equals the sum of those in Exp2 and Exp3.

The following, more general statement, is an EBM counterpart of the mechanism hypothesized in the introduction: *Polar amplification will always be seen in an EBM if (1) the sensitivity, B , of the TOA budget to SST perturbations is fixed at a uniform value, and (2) the diffusion coefficient in the heat transport parameterization increases with SST, thus mimicking the increase in meridional latent heat transport.* If we apply an external (ghost) forcing to such a system the imbalance at the surface will force the SST to rise, uniformly in the beginning. This leads to an increase in the lateral heat transport from the tropics to the extra-tropics. This heat input to the extra-tropics will be larger than what can be lost to space, since the TOA sensitivity is uniform and it was assumed that the SST had risen uniformly. The extra heat at high latitudes will lead to a higher local SST increase which allows the TOA to release more

energy from the system. In turn, this reduces the energy transport from the tropics and the system can eventually equilibrate. Hence, the only way an EBM with the above mentioned properties can respond to the 4 W/m^2 forcing is the pattern with higher SST increases at high latitudes. The more sensitive the horizontal energy transport is to the increase in SST, the more pronounced the polar amplification.

3 GCM experiments

3.1 Model description

Two different models, with completely different physics and dynamics packages, are used in order to demonstrate the robustness of the hypothesized mechanism. They are run at comparable horizontal and vertical resolutions, on aquaplanets and without the seasonal cycle; “modified equinox” conditions as described in A03 are employed.

Model 1 is the Goddard Space Flight Center GEOS model as used and described in A03. It is run at $4^\circ \times 5^\circ$ horizontal resolution with 20 layers in the vertical. The clouds have been zeroed out in the radiation code.

Model 2 is the National Center for Atmospheric Research CCM 3.6.6 run at T42 horizontal resolution with 18 vertical levels (described by Kiehl et al. 1996). Our modifications to the standard distribution of this model are described in Langen and Alexeev (2004). One extra modification here is the absence of the ice-albedo feedbacks, similar to what was used in A03: the surface albedo is constant and uniform everywhere and points where the SST drops below freezing are treated as water points. All effects of clouds are kept in the code and the solar constant and CO_2 concentration are set to the CCM3 default values of $1,367 \text{ W/m}^2$ and 355 ppm, respectively.

A mixed-layer model (of depth $H = 50$ m) is coupled to the atmospheric part in both models via the surface heat budget, and the tendency equation for the surface temperature, T_s , is in each grid point given by:

$$\rho_w c_w H \frac{\partial T_s}{\partial t} = F_S - F_I - F_H - F_L (+G), \quad (3)$$

where ρ_w and c_w are the density and heat capacity of sea water, respectively, and F_S , F_I , F_H and F_L , designate the net downward shortwave, the net upward longwave and the sensible and latent heat fluxes. The term G added in parenthesis on the right hand sign demonstrates how the ghost forcing is inserted into the mixed-layer. The two models are run until they reach a quasi-steady state, the time average of which is then considered the equilibrium climate. The uniform surface albedo of Model 1 was tuned to 0.225 to yield a present-day-like SST profile, and that of Model 2 was then tuned to 0.05 to give a similar profile. The equi-

librium climates, shown in Fig. 4a, were then perturbed by doubling the CO_2 concentration in the physics package. After running the two models long enough for equilibration the polar amplification patterns displayed in Fig. 4b were found. For completeness, we repeat in Fig. 5a these polar amplification patterns along with those obtained when running Model 1 *with* clouds (surface albedo 0.15) and Model 2 *without* clouds (surface albedo 0.18). Panel (b) shows the same curves scaled by their tropical mean SST increase to facilitate comparison of the actual polar amplification. Clouds in both models are seen to strengthen the polar amplification but are not solely responsible for it. While the cloud feedbacks giving these effects are interesting and worth further investigation, they are not within the scope of the present study. We have, in fact, chosen the two very different model configurations described above (giving the two extremes in Fig. 5b) to illustrate that the same mechanism is at play in both.

3.2 Ghost forcing

Figure 6 shows the result of the three ghost forcing experiments (Table 1) with the two GCMs. The forcing has simply been inserted directly into the tendency equation for the mixed layer temperature and thus has no direct physical counterpart such as greenhouse gas or insolation changes. The first thing to notice is that the responses look qualitatively similar. The tropical-only forcing (Exp2) gives a very non-local, almost uniform, response, while the response to the extra-tropical-only forcing (Exp3) is stronger locally than in the tropics.

As is seen in Fig. 6, the sum of the responses in Exp2 and Exp3 almost coincides with the response obtained in Exp1. This implies that there is a certain degree of linearity of our systems’ SSTs with respect to the surface forcing. This linearity turns out to be a very convenient feature allowing a decomposition of the response to the uniform global surface forcing into the responses to the

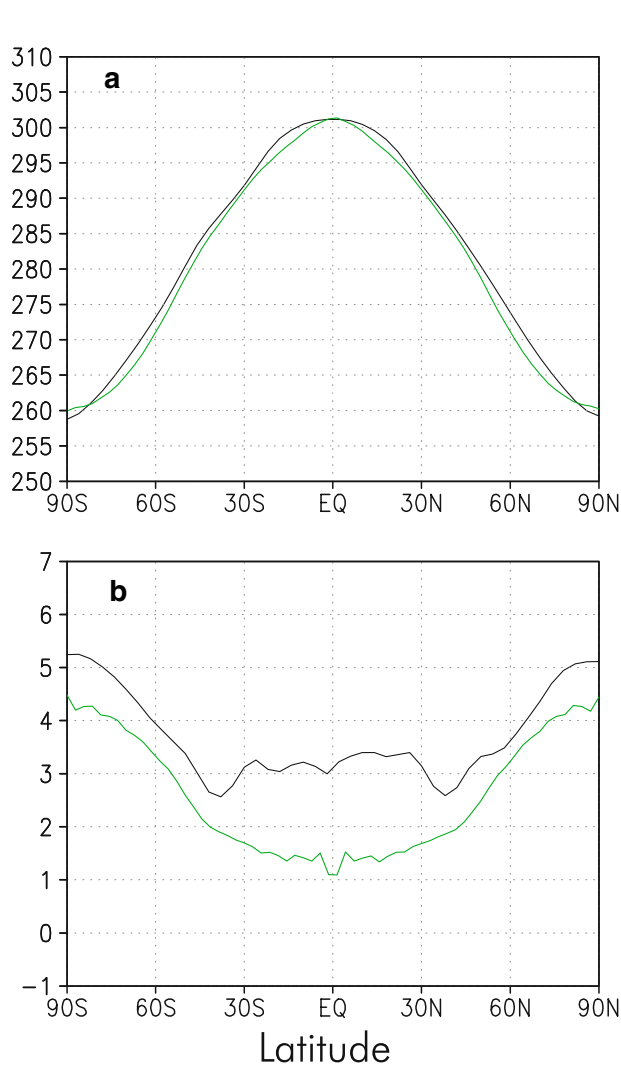


Fig. 4 **a** Equilibrium $1\times\text{CO}_2$ SSTs as function of latitude, Model 1 (black) and Model 2 (green). **b** Difference between $2\times\text{CO}_2$ and $1\times\text{CO}_2$. Units are K

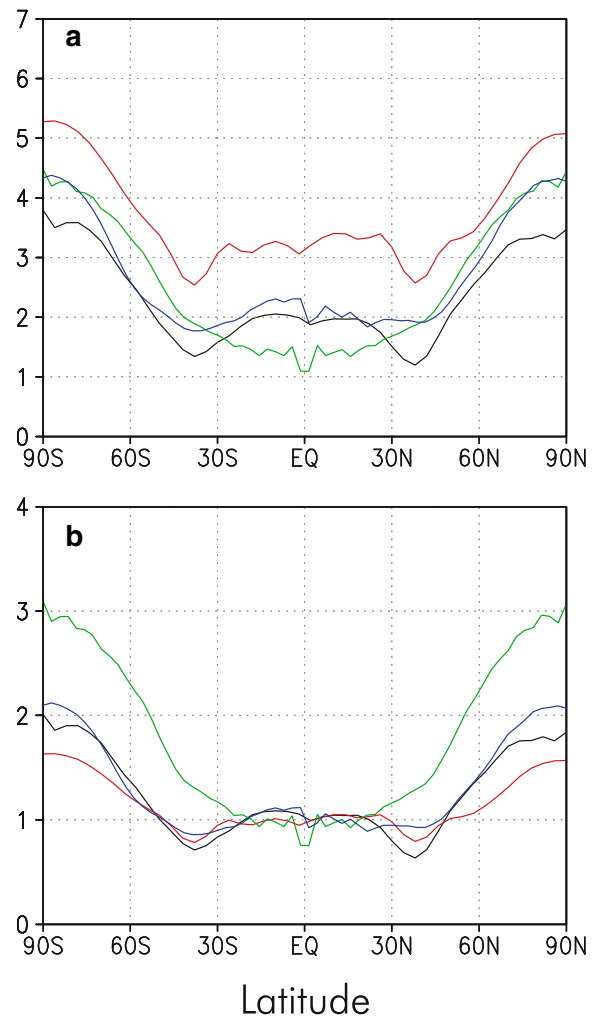


Fig. 5 **a** SST change resulting from a doubling CO_2 in Model 1 with clouds (black) and without clouds (red) and in Model 2 with clouds (green) and without clouds (blue). **b** As in panel (a) but with changes normalized by their tropical mean value. Units in panel (a) are K while panel (b) is non-dimensional

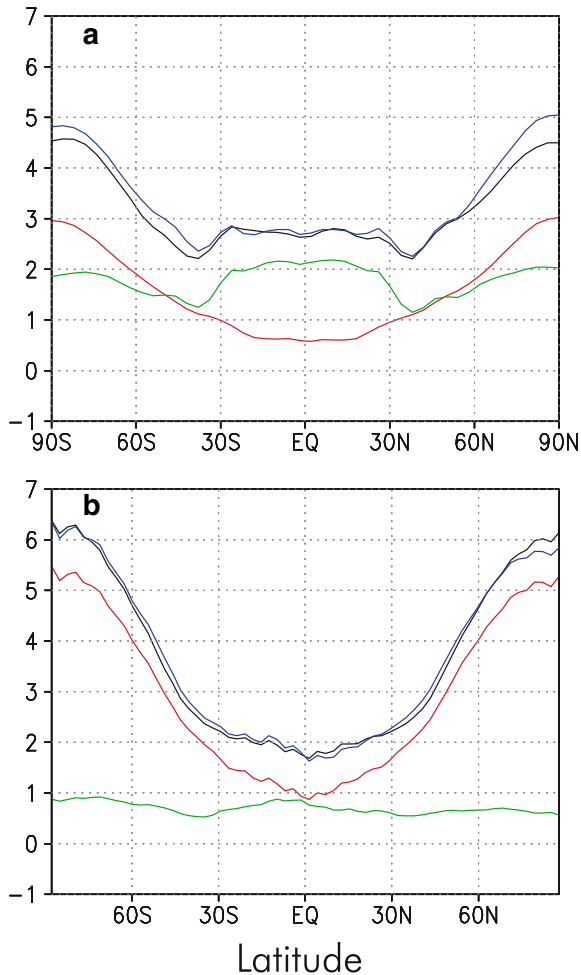


Fig. 6 **a** Response of Model 1 to uniform 4 W/m^2 ghost forcing (black), to the tropical-only ghost forcing (green) and to the extra-tropical-only ghost forcing (red); sum of responses to the tropical-only and extra-tropical-only forcings (blue). **b** As in (a), but for Model 2. Units are K

tropical- and extra-tropical-only forcings. By applying this analysis the importance of the local high-latitude SST response can be compared to the remote response from the tropics. For Model 1, the “local” contribution to the warming at the poles amounts to 3 K, while the non-locality, with 2 K, is almost as important as the local response. For Model 2, the total polar increase of 6 K is the sum of a much larger local contribution of 5 K and a non-local contribution of 1 K.

The greater polar warming can thus be explained as a superposition of a strong local response to the extra-tropical forcing and a remote response to the tropical-only forcing. Without the non-local response at high latitudes to the tropical forcing the pattern of the amplification would have been less pronounced. In fact, if there had not been a mechanism for communicating the tropical forcing to higher latitudes, the tropical response might have been considerably larger and the polar amplification significantly reduced.

3.3 Forcing and response in $2\times\text{CO}_2$ and ghost forcing experiments

Figure 7 shows the total surface forcing in the two models resulting from the doubling of CO_2 , i.e., the net surface imbalance obtained in a run with fixed equilibrium $1\times\text{CO}_2$ SST and doubled CO_2 concentration in the atmosphere. Again, the two models give qualitatively similar results: the maximum of the forcing is located over the tropics and its magnitude becomes smaller at high latitudes. The area averages over the tropics look similar for the two models, ca. 5.5 and 4 W/m^2 , but at higher latitudes the value in Model 2 is smaller than that in Model 1 by almost a factor of two. The 4 W/m^2 used for the uniform ghost forcing is therefore quite close to the actual CO_2 forcing in Model 1 and the responses from the CO_2 forcing (Fig. 4b) and the ghost forcing (Fig. 6a) are also remarkably similar. In Model 2, however, the CO_2 forcing is not very well approximated by the uniform ghost forcing, but given the linearity of the model’s response, the numbers in Fig. 4b can roughly be inferred from Figs. 6b and 7: at high latitudes the CO_2 gives only half the forcing of 4 W/m^2 and the local response is $1/2\times 5 \text{ K}$. Added to the 1 K increase from the low-latitude forcing of 4 W/m^2 this gives 3.5 K (compare with 4 K in Fig. 4b). At low latitudes, the local forcing of 4 W/m^2 gives 1 K while the high-latitude forcing gives $1/2\times 1 \text{ K}$. The sum of 1.5 K compares well with the equatorial warming seen in Fig. 4b.

The uniform 4 W/m^2 forcing results in global average SST increases of 2.8 and 2.9 K in Models 1 and 2, respectively. The global average sensitivity is thus approximately $0.7 \text{ K}/(\text{W/m}^2)$ in both models. The responses to the CO_2 doubling results in the rather different global average warmings of 3.3 and 2.1 K. The surface forcings are, however, also quite different,

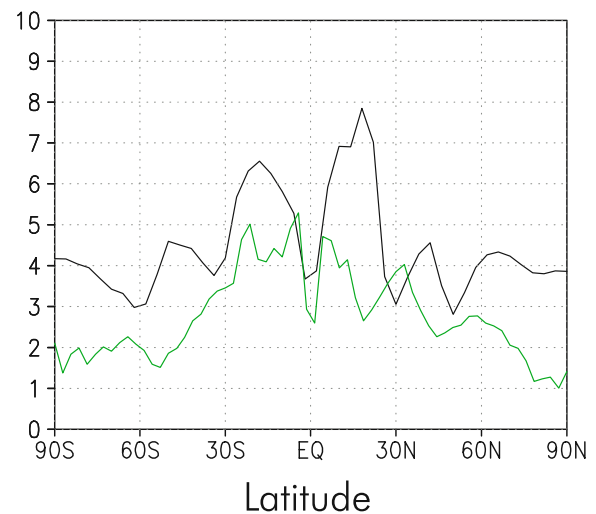


Fig. 7 Total dynamic-radiative surface forcing as a result of doubling the CO_2 concentration while keeping the SST fixed at the equilibrium value, Model 1 (black), Model 2 (green). Units are W/m^2

namely 4.8 W/m^2 and 3.2 W/m^2 , and the sensitivities are here $0.7 \text{ K/(W/m}^2)$ and $0.65 \text{ K/(W/m}^2)$. The reduced sensitivity in Model 2 stems from the manner in which the 3.2 W/m^2 was imposed: it had most of its weight at low latitudes, while Fig. 6b shows that adding heat to high latitudes much more efficiently increases the global average SST.

3.4 Fixed SST

The tropical part of a surface forcing creates a near-uniform global warming. The fact that an equatorially amplified pattern is not produced hinges on the mechanism described in the introduction: a tropical warm anomaly increases the poleward heat transport which warms and moistens the high-latitude atmosphere. This change produces a positive forcing on the high-latitude surface budget. This will be demonstrated in the present subsection with fixed SST anomalies confined to regions corresponding to those forced in the above experiments. The idea is to simulate a situation where the SST responds to the ghost forcings “locally” and thus obtain a picture of the initial imbalances and transports in the ghost forcing experiments.

Applying a tropical-only forcing will initially result in a temperature perturbation with a shape roughly as shown in Fig. 8. Since this SST anomaly is a result of the tropical forcing, there is a mechanism sustaining it and it can be assumed that the perturbation will have a relatively long time scale. To quantify the non-locality of the response of the surface budget to such an SST anomaly, experiments with SST fixed at the equilibrium profile and perturbed by the described tropical SST anomaly were run. The perturbed surface budget with its components is shown in Fig. 9. A pronounced local response in the tropical surface budget is seen and, importantly, there is a significant non-zero imbalance over the areas where the SST perturbation was zero. The sign of the

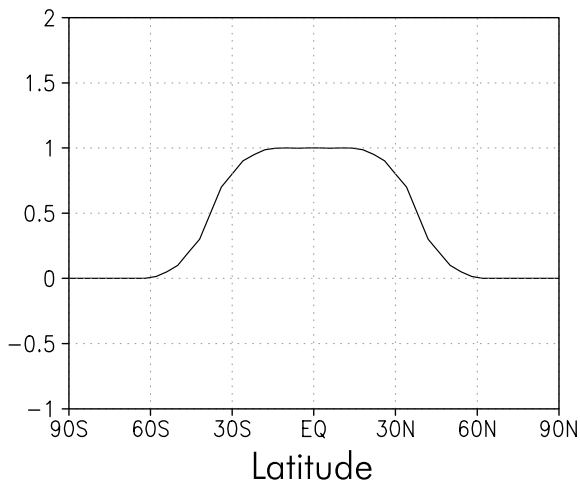


Fig. 8 SST perturbation used in “tropical-only” perturbation experiment. Units are K

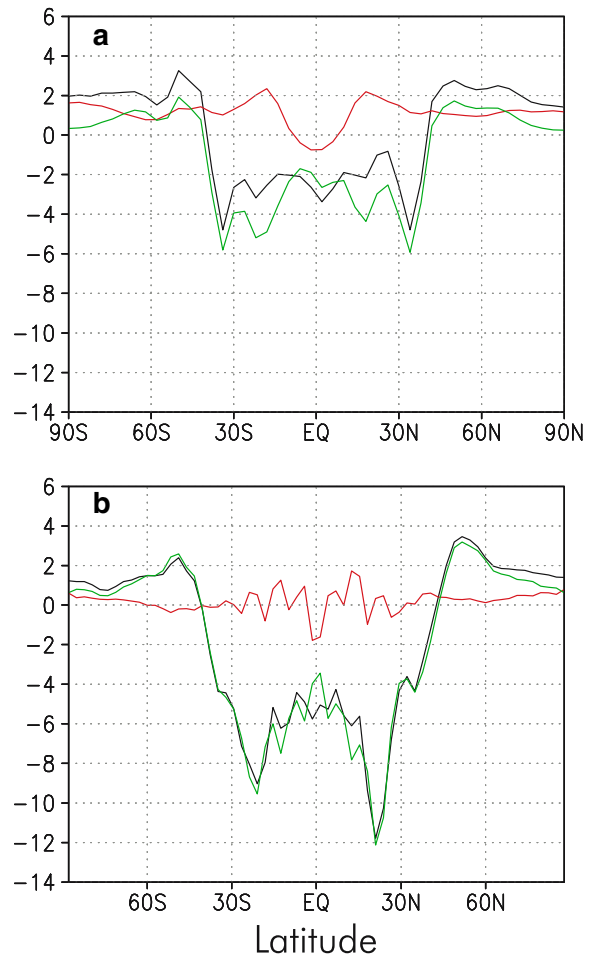


Fig. 9 **a** Equilibrium response to the fixed “tropical-only” SST anomaly of the total surface budget of Model 1 (*black*), turbulent fluxes (LH + SH, *green*), radiative fluxes (*red*). **b** as in (**a**), except for Model 2. Units are W/m^2

surface heat budget anomaly is positive at high latitudes (ca. 2 W/m^2 for Model 1, ca. 1.6 W/m^2 for Model 2), and thus creates a net warming tendency on the SST there. Hence, if there were a persistent tropical SST anomaly in our model, the resulting tendency on the SST at high latitudes would be a warming.

Closer inspection of the composition of the tendency shows that the LW contribution is the most important near the poles for Model 1, and that for Model 2 the radiative and turbulent fluxes are of comparable magnitudes (ca. 0.6 and 1 W/m^2 , respectively). This can be explained by looking at the green curves in Figs. 11 and 12, showing the temperature and specific humidity responses at 80N to the tropical temperature anomaly. In Model 1, the responses vanish at the very surface and the forcing must be radiative in origin. In Model 2, however, the lowest atmospheric layer displays increases in temperature and humidity which both inhibit the turbulent heat loss and thus augment the radiative tendency from the higher layers.

In addition to the tropical SST perturbation experiment, two other perturbation experiments were per-

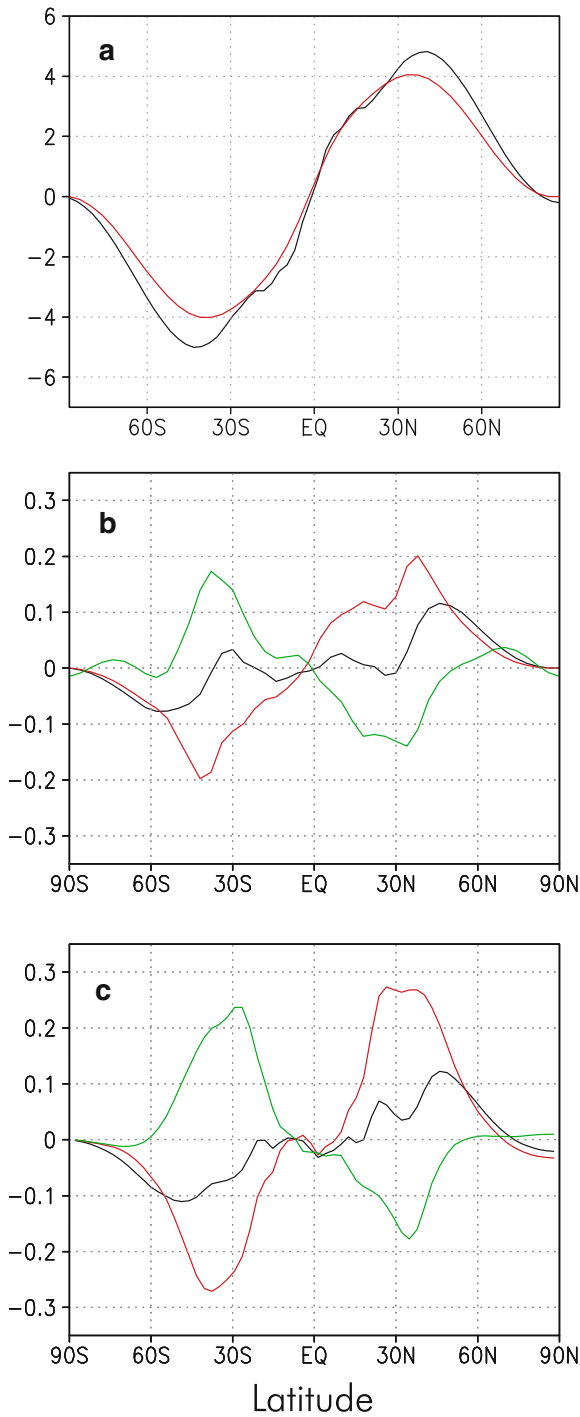


Fig. 10 **a** The TOA and surface heat budget implied total atmospheric meridional heat transport in the equilibrium fixed SST experiment for Model 1 (*red*) and Model 2 (*black*). **b** Change in heat transport in the fixed uniform (*black*), tropical (*red*) and extra-tropical (*green*) SST perturbation experiments for Model 1. **c** As in panel (**b**) but for Model 2. Units are PW

formed: in one, the equilibrium SST was increased uniformly by 1 K and in the other the SST perturbation represents an “extra-tropical-only” perturbation, namely the difference between a uniform 1 K perturbation and the one from Fig. 8. Figure 10a shows the

meridional atmospheric heat transport as implied by the difference between the TOA and surface heat budgets in the fixed equilibrium SST run for both models while panels (**b**) and (**c**) show the transport changes in the uniform (*black*), tropical (*red*) and extra-tropical (*green*) perturbation experiments for both models, respectively. The changes in the transports are much like one would expect from the EBM picture outlined previously: when the temperature is increased uniformly the gradients do not change but the atmosphere warms and transports more energy. When only the tropical SSTs are increased this effect is augmented by the effect of the increased gradient to lead to an even larger increase in transport. When only the extra-tropics are warmed the two effects compete and the net result turns out to be a decrease in the transport.

Figures 11 and 12 display the changes in the temperature and specific humidity profiles at 80N resulting from the changes in surface temperature and heat transport. Despite the fact that the physics packages are independent and that cloud effects are excluded from the

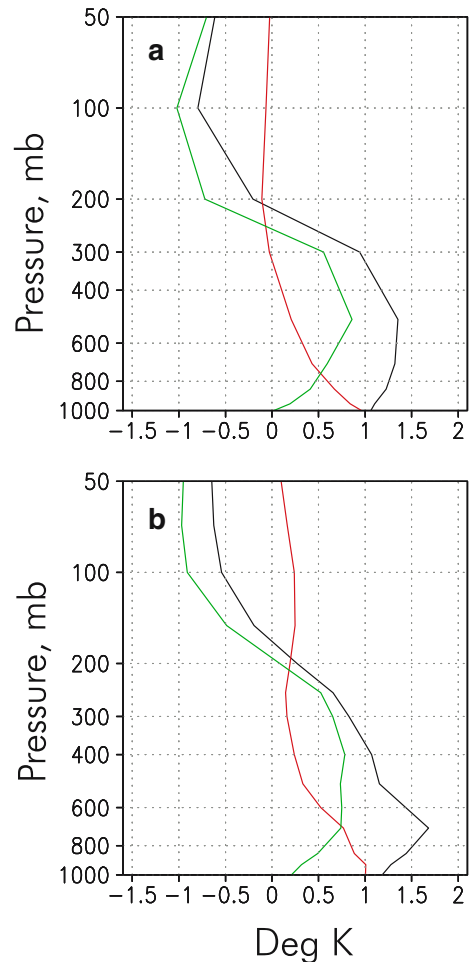


Fig. 11 **a** Temperature response at 80N for Model 1 in uniform 1 K SST perturbation experiment (*black*), tropical-only 1 K SST perturbation (*green*) and extra-tropical-only 1 K SST perturbation experiments (*red*). **b** As in (**a**), but for Model 2. Units are K

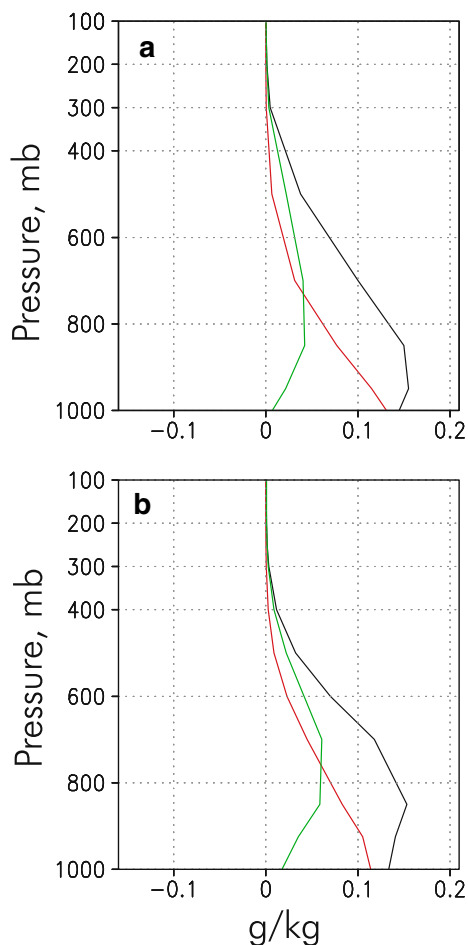


Fig. 12 As in Fig. 11, but for specific humidity. Units are g/kg

radiation code of Model 1, the temperature and specific humidity responses to the perturbations look surprisingly similar in the two models. Again, linearity in the responses holds with relatively high accuracy. The response to the extra-tropical SST anomaly is relatively shallow compared to those of the uniform and tropical-only SST perturbations. In fact, the temperature response in the tropical-only perturbation experiment is actually stronger at altitudes higher than ca. 750 hPa. The response in the specific humidity looks very similar to that of temperature in all three experiments, and these responses are, as discussed, the reason for the remote response of the surface budget in the tropical-only SST perturbation experiments. While the temperature increase arises due to the increased heat transport, it is unclear whether the moisture change is remote or local in origin. The latent heat transport has increased but due to the continuous recycling of moisture along the trajectories it is hardly discernible whether the moisture was imported to the high latitudes or if it was evaporated locally. More directly, the warmer polar atmosphere can, according to the Clausius–Clapeyron relation, hold more water vapor, and the free tropospheric water vapor feedback (as studied by e.g.

Schneider et al. 1999) thus plays a part in producing the polar amplification by enhancing the longwave effect on the surface.

We have not shown the surface budget response to the extra-tropical SST perturbation but it displays, as expected, a local (high-latitude) cooling tendency. This tendency is, however, significantly smaller than the tropical cooling tendency in response to the tropical perturbation. Hartmann (1994) has demonstrated that the non-linearity of the Clausius–Clapeyron relationship renders the latent cooling more sensitive to perturbations in the warm tropics, and this difference in sensitivities further contributes to forming the polar amplification pattern (a topic that has been further studied by Bates (2003)). As is evident in Fig. 9, Model 2 produces a much stronger local surface budget response to the tropical SST anomaly than Model 1, which means that it does not need to warm as much in the tropics to counter an applied forcing. This effect contributes to the stronger polar amplification in Model 2 and is consistent with the climate model intercomparison finding that the CCM3 is among the least sensitive models in terms of its $2\times\text{CO}_2$ global SST response (Covey et al. 2003).

3.5 1D estimates with the CCM

To determine the relative influences of the changes in temperature and moisture (and clouds in Model 2) in producing the LW forcing at the high-latitude surface the single column CCM radiation code was employed. First, the 1D radiation code was run with vertical profiles of moisture and temperature from the corresponding equilibrium climates for both models. The equilibrium profiles were then perturbed locally at 80N by the anomaly obtained in the “tropical-only” SST perturbation experiment.

Three different experiments were conducted for Model 1: (1) With perturbed temperature and moisture fields, (2) with perturbed temperature and unperturbed moisture and (3) with perturbed moisture and unperturbed temperature fields. The anomalies in the radiative fluxes obtained in the latter two experiments add up linearly to the anomaly of ca. 1.5 W/m^2 , obtained in the former experiment. The temperature perturbation contributes with ca. 1.1 W/m^2 to the total 1.5 W/m^2 perturbation.

For Model 2, profiles of cloudiness and cloud liquid water path were also collected and used along with temperature and moisture as for Model 1. Additionally, the cloud ice fraction was fixed to avoid inconsistencies when comparing experiments with different temperature and moisture perturbations. The results are presented in Table 2 and are again linear with respect to the various perturbations, i.e., the sum of “ T ” and “ q ” matches closely “ T and q ”. The same applies for the cloud variables and the sum of “ T and q ” and “ Cld and Lwp ” is almost “ All ”. This linearity permits us to determine the relative importance of the various perturbations.

Table 2 Changes in SW and LW components at 80N (in W/m^2) for different perturbation profiles in 1D local diagnostic runs. “Ref” is the reference case while, for example, “ T ” means that the temperature profile from the perturbation experiment is used while all

other profiles are taken from the equilibrium run. “ T and q ” means that perturbation profiles are used for both temperature and moisture. “All” means that all of the profiles are taken from the perturbation experiment

Δ (Wm^{-2})	Ref	T	q	T and q	Cld	Lwp	Cld and Lwp	All
SW (+ve down)	0.0	0.018	-0.082	-0.065	-0.199	-0.303	-0.504	-0.567
LW (+ve up)	0.0	-0.495	-0.161	-0.655	-0.217	-0.409	-0.619	-1.273
Net (+ve down)	0.0	0.511	0.078	0.589	0.016	0.105	0.114	0.705

As for Model 1, it is found that the temperature perturbation dominates over the moisture perturbation in producing the surface forcing. It also dominates over the cloud effects. In fact, the relative influences of temperature, moisture and clouds are given roughly by the ratio 5:1:1 (compare with 3:1 for temperature and moisture in Model 1). The two different cloud variables clearly yield significant responses, but their combined SW and LW effects tend to cancel. Taking this cancellation into account, it is concluded that the bulk of the forcing stems from the LW effect due to the temperature perturbation, and even when clouds are included in the model the LW forcing due to the tropical SST anomaly is produced in the same qualitative manner.

4 Discussion and conclusions

To explain the polar amplification pattern obtained on an aquaplanet with no ice-albedo feedback, we analyze the behavior of the system in more physical terms than was done in A03. Three different models have been used: an EBM and two full 3D atmospheric GCMs which are run with no seasonal cycle and no ice-albedo feedback, and are coupled to aquaplanet upper mixed-layer models. The two GCMs differ significantly: they have completely different physics and dynamics packages and one model includes the effects of clouds while the other does not. While cloud feedbacks have not been within the scope of the present study, Fig. 5 showed that clouds play a significant role in determining both the magnitude and shape of the warming due to an increase in atmospheric CO_2 . In the models employed here, they seem to enhance the polar amplification without being a prerequisite for it. In the detailed studies of the GCMs, one was run with and the other without clouds and the mechanism responsible for the pattern was identified to be the same in both models.

In the simple framework of the EBM it was demonstrated that with heat transports depending only on meridional temperature gradients the model does not produce polar amplification without the ice-albedo feedback. When a crude representation of the increase in atmospheric heat transport in a warmer atmosphere was introduced, an amplification was seen even with equal low and high-latitude sensitivities of the outgoing longwave radiation ($B=2 W/m^2$). A uniform forcing initially increases the temperature uniformly leading to an increased meridional heat transport. This initial increase

in heat transport causes the extra-tropics to warm more than the tropics under the uniform forcing.

This mechanism was demonstrated also to be active in the GCMs in fixed SST experiments and three different “ghost forcing” experiments (Hansen et al. 1997), in which extra energy was inserted into the mixed layer. The first one consisted of $4 W/m^2$ uniformly distributed over the globe, in order to roughly simulate the $2\times CO_2$ forcing at the surface. The second and third forcings, of the same magnitude, were applied only to the tropics and extra-tropics, respectively. The systems’ equilibrium responses were found to be linear with respect to these forcings in that the sum of responses to the tropical and extra-tropical forcings practically coincides with the response to the uniform forcing, the latter resembling our earlier results obtained in $2\times CO_2$ experiments. The polar amplification can thus be viewed as a sum of the essentially non-local response to the tropical forcing and the more local and higher amplitude response to the extra-tropical forcing.

The uniformity of the response to the tropical forcing comes about for several reasons. Firstly, a uniform or equatorially amplified response leads to an increase in the poleward heat transport which warms and moistens the high-latitude atmosphere. These changes are amplified by the free tropospheric water vapor feedback and lead to longwave warming of the high-latitude surface which has also been seen in studies by Schneider et al. (1997, 1999) and Rodgers et al. (2003). The increase in heat transport is, as mentioned, seen during a uniform or equatorially amplified temperature increase and thus excludes the possibility of the final response having such shapes. When equilibrium is reached, however, the polar amplification will have decreased meridional temperature gradients enough to weaken, and perhaps even counter, the increase in transport. This is why such a study of the polar amplification must necessarily address the conditions during the transients—as was done with our fixed SST and ghost forcing experiments. A straightforward comparison of the $1\times CO_2$ and $2\times CO_2$ equilibria would not have provided us with these insights.

The increase in poleward heat transport with global mean temperature, which has been shown to play a key role for the polar amplification, seems to be a rather robust result for the present-day-like climates studied here. Caballero and Langen (2005) have, however, demonstrated that the heat transport may saturate in warmer, low-gradient climates. The present mechanism

thus yields a polar amplification in a warming from present conditions, but is, according to the cited study, unlikely to explain the equable climates of the Earth’s past.

A second reason for the uniformity of the response to low-latitude forcing and thus, in turn, the polar amplification is to be found in differences in the surface budgets to SST changes at low and high latitudes. The tropical surface budget is more sensitive to SST changes than that of the extra-tropics, and thus needs smaller changes in SST to counter the imposed forcing.

The strong stratification of the high-latitude troposphere tends to confine the temperature change in, for example, a $2\times\text{CO}_2$ experiment to the very lowest atmospheric layers (e.g. Manabe et al. 1991, 1992). After ice-albedo feedbacks, this has been put forth to be the most important reason for the polar amplification (e.g., Hansen et al. 1997), but our tropical SST perturbation experiments suggest that such a local cause-and-effect relationship between the forcing and the response in lapse rate is insufficient: through the large-scale circulation, the high-latitude troposphere feels the tropical SST and produces a longwave forcing on the high-latitude SST which changes and, in turn, affects the local lapse rate.

We note that the surface ghost forcing technique is quite straightforward to implement in any model, including fully coupled 3D OA-GCMs with sea ice of any complexity. The present study could thus be considered as an application of the proposed technique to the diagnosis of the polar amplification in the two models, with possible future applications in more complex climate system models.

Acknowledgements The work was supported by IARC/NSF Cooperative Agreement 330360-66900 and the University of Copenhagen. The authors would like to thank R. Caballero for useful discussions, the CAM-user group for answering questions about the 1D CCM radiation model, and E. Schneider and an anonymous reviewer for suggestions and comments that have led to significant improvements of the manuscript.

References

- Alexeev VA (2003) Sensitivity to CO_2 doubling of an atmospheric GCM coupled to an oceanic mixed layer: a linear analysis. *Clim Dyn* 20:775–787
- Alexeev VA, Bates JR (1999) GCM experiments to test a proposed dynamical stabilizing mechanism in the climate system. *Tellus* 51A:630–651
- Bates JR (1999) A dynamical stabilizer in the climate system: a mechanism suggested by a simple model. *Tellus* 51A:349–372
- Bates JR (2003) On climate stability, climate sensitivity and the dynamics of the enhanced greenhouse effect. DCESS Report No.3, available from Department of Geophysics, University of Copenhagen <http://www.dclimate.gfy.ku.dk>
- Bellon G, Le Treut H, Ghil M (2003) Large-scale and evaporation-wind feedbacks in a box model of the tropical climate. *Geophys Res Lett* 30(22, Art. no. 2145)
- Caballero R, Langen PL (2005) The dynamic range of poleward energy transport in an atmospheric general circulation model. *Geophys Res Lett* 32:L02705. DOI: 10.1029/2004GL021581
- Chen D, Gerdes R, Lohmann G (1995) A 1-d atmospheric energy balance model developed for ocean modeling. *Theor Appl Climatol* 51:25–38
- Covey C, AchutaRao KM, Cubasch U, Jones P, Lambert SJ, Mann ME, Phillips TJ, Taylor KE (2003) An overview of results from the Coupled Model Intercomparison Project. *Glob Planet Change* 37:103–133
- Flato GM, Hibler WD (1992) Modeling pack ice as a cavitating fluid. *J Phys Oc* 22:626–651
- Hall A (2004) The role of surface albedo feedback in climate. *J Clim* 17:1550–1568
- Hansen J, Sato M, Ruedy R (1997) Radiative forcing and climate response. *J Geophys Res* 102(D6):6831–6864
- Hartmann DL (1994) *Global physical climatology*. Academic, New York
- Hibler WD (1985) Modeling sea-ice dynamics. *Adv Geophys* 28:549–579
- Houghton JT et al (eds) (2001) *IPCC, Climate: the scientific basis*. Cambridge University Press, Cambridge
- Kiehl JT, Hack JJ, Bonan GB, Boville BA, Briegleb BP, Williamson DL, Rasch PJ (1996) Description of the NCAR Community Climate Model (CCM3). Technical Report TN-420, CGD, National Center for Atmospheric Research
- Langen PL, Alexeev VA (2004) Multiple equilibria and asymmetric climates in the CCM3 coupled to an oceanic mixed layer with thermodynamic sea ice. *Geophys Res Lett* 31. DOI: 10.1029/2003GL019039
- Manabe S, Stouffer RJ, Spelman MJ, Bryan K (1991) Transient responses of a coupled ocean–atmosphere model to gradual changes in atmospheric CO_2 . Part I: annual mean response. *J Clim* 4:785–818
- Manabe S, Spelman MJ, Stouffer RJ (1992) Transient responses of a coupled ocean–atmosphere model to gradual changes in atmospheric CO_2 . Part II: seasonal response. *J Clim* 5:105–126
- North GR (1975) Analytical solution to a simple climate model with diffusive heat transport. *J Atmos Sci* 32:1301–1307
- Polyakov IV, Alekseev GV, Bekryaev RV, Bhatt U, Colony RL, Johnson MA, Karklin VP, Makshtas AP, Walsh D, Yulin AV (2002) Observationally based assessment of polar amplification of global warming. *Geophys Res Lett* 29(18):1878
- Rodgers KB, Lohmann G, Lorenz S, Schneider R, Henderson GM (2003) A tropical mechanism for Northern Hemisphere deglaciation. *Geochem Geophys Geosyst* 4(5):1046. DOI:10.1029/2003GC000508
- Sarachik ED (1978) Tropical sea surface temperature: an interactive one-dimensional atmosphere-ocean model. *Dyn Atmos Oceans* 2:455–469
- Schneider EK, Lindzen RS, Kirtman BP (1997) A tropical influence on global climate. *J Atm Sci* 54:1349–1358
- Schneider EK, Kirtman BP, Lindzen RS (1999) Tropospheric water vapor and climate sensitivity. *J Atm Sci* 56:1649–1658
- Shine KP, Cook J, Highwood EJ, Joshi MM (2003) An alternative to radiative forcing for estimating the relative importance of climate change mechanisms. *Geophys Res Lett* 30(20), 2047. DOI:10.1029/2003GL018141
- Sokolov AP, Stone PH (1998) A flexible climate model for use in integrated assessments. *Clim Dyn* 14:291–303
- Vavrus SJ (2004) The impact of cloud feedbacks on arctic climate under greenhouse forcing. *J Clim* 17:603–615
- Vavrus SJ, Harrison SP (2003) The impact of sea ice dynamics on the arctic climate system. *Clim Dyn* 20. DOI:10.1007/s00382–003–0309–5
- Walsh JE, Kattsov VM, Chapman WL, Govorkova V, Pavlova T (2002) Comparison of arctic climate simulations by uncoupled and coupled global models. *J Clim* 15(12):1429–1446